Journal of Sound and Vibration (2001) **240**(1), 87–115
doi:10.1006/jsvi.2000.3188, available online at http://www.idealibrary.com on IDEAL®

VIBRATION CONTROL IDENTIFICATION OF SEISMICALLY EXCITED m.d.o.f. STRUCTURE-PTMD SYSTEMS

C.-C. Lin, J.-F. Wang and J.-M. Ueng

Department of Civil Engineering, National Chung-Hsing University, Taichung, Taiwan 40227, *Republic of China. E-mail: cclin3@dragon.nchu.edu.tw*

(*Received* 10 *January* 2000, *and in final form* 3 *July* 2000)

In this paper, the vibration control philosophy and optimal design of passive tuned mass dampers (PTMDs) for a multi-degree-of-freedom (m.d.o.f.) structure are presented. In order to prove the effectiveness of PTMD, the modal properties of a m.d.o.f. building with an optimal PTMD are identified using a specified system identification procedure. The difference in the modal properties between a structure with and without PTMD determines the PTMD vibration control performance. An extended random decrement method, which considers the measurement correlation, was first employed to reduce the measured dynamic responses of the building. The Ibrahim time domain technique was then applied to calculate the modal frequencies, damping ratios, and mode shapes based on only a few floor response measurements. To obtain the complete mode shapes, an interpolation method was developed to estimate the mode shape values for the locations without measurements. The seismic responses at floors with and without measurements were also calculated. Numerical results throughout a five-storey building under ambient random excitations demonstrated that the proposed system identification techniques are able to identify the dominant modal parameters of the system accurately, even with high closed-space frequencies and noise contamination. In addition, PTMD was proved to be a useful control device.

1. INTRODUCTION

Due to recent intensive analytical and experimental research, vibration control in structures using passive tuned mass dampers (PTMDs) is gaining more acceptance not only in the design of new structures and components but also in the retrofit of existing structures to enhance their reliability against winds, earthquakes and human activities [1–5]. PTMDs can be incorporated into an existing structure with less interference compared with other passive energy dissipation devices. Since 1971, lots of PTMDs have been successfully installed in high-rise buildings and towers such as the Citicorp Center in New York City and John Hancock Tower in Boston, USA, and Crystal Tower and the Higashiyama Sky Tower, Chiba Port Tower and Fukuoka Tower in Japan. All these retrofits were reported to be able to significantly reduce structural dynamic response.

Basically, a PTMD is a device consisting of a mass connected to structures using a spring and a viscous damper, as shown in Figure 1. The determination of PTMD system parameters is the main issue in the study of PTMD. Several optimization procedures have been proposed by many researchers in the past decades. In conventional mathematical derivations, the equations of motion of entire system of PTMD-structure were separated into those for PTMD and the primary structure. Through modal analysis, according to the

0022-460X/01/060087 + 29 $35.00/0

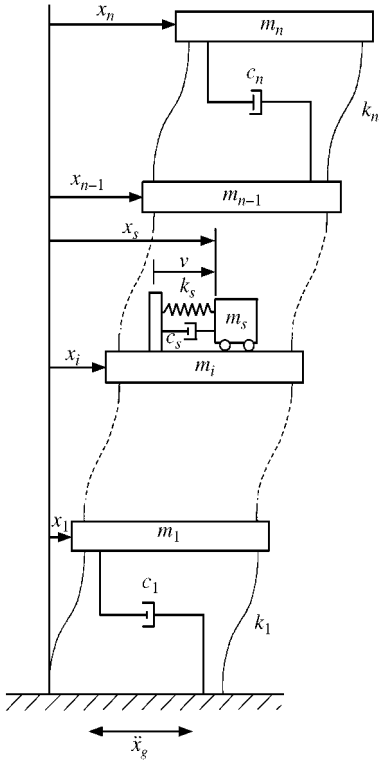

Figure 1. System model of multi-storey building structure with single PTMD.

modal parameters of the primary structure, the optimum PTMD parameters can be carried out by optimizing a prescribed effectiveness index in the frequency domain [6–10]. In recent years, different approaches for the PTMD optimal design have been proposed. Tsai [11] and Fujino and Abe [12] calculated the parameters of PTMD based on perturbation techniques. Sadek *et al.* [13] extended the work of Villaverde [14] to find the tuning parameters by making the first two modal damping ratios of the PTMD-structure system equal. Hadi and Arfiadi [15] utilized the active-control concepts to establish the optimization criteria. The H_2 norm of the transfer function from the external disturbance to a certain regulated output was taken as a performance measure of the optimization criterion. Then, the genetic algorithm, which has been successfully applied in many applications, is used to find the optimum PTMD parameter value. More recently, an innovative work was presented by Carott and Turci [16], who used a well-established mathematical idiom, rotating vectors in the Argand–Gauss plane, to design the PTMD parameters. This approach attained the same result as the classical theory, but with the advantage of providing a succinct description of the phase and magnitude relationships between the primary structure and the PTMD.

Although the previous studies on PTMD were abundant, its vibration control effectiveness is still controversial, especially for seismic applications [17]. For example, Xu and Kwok [18] found that the efficacy of PTMD was not as good as expected based on a wind tunnel test of a tall building subjected to along, cross and torque wind excitations. Villaverde [19] investigated the PTMD effectiveness through three different structures subjected to nine actual earthquake records. He found that PTMD had good performance

in some cases, but some had little or even no effect. However, Sadek *et al*. [13] did the same study for 30 single-degree-of-freedom (s.d.o.f.) structures with periods between 0·1 and 3·0 s under 52 real earthquakes. The comparisons of mean structural responses with and without PTMD indicate that PTMD is effective. Above inconsistency mainly resulted from using different dynamic characteristics of structure and external excitation, and different performance measures to determine the PTMD effectiveness. The idealization of external force in PTMD design stage is a problem which needs further study.

The PTMD damping effect depends upon the fact that the PTMD response delays the main structural response by a phase angle of 90°, so that the elastic force transmitted by the PTMD acts like a viscous force on the main structure. This condition will not occur unless the PTMD frequency is tuned to the frequency of the main structure and the excitation has this frequency content. Therefore, the structural property information is very essential for the optimum design of a PTMD. Meanwhile, the PTMD detuning effect should be seriously investigated. Tsai [11] derived the explicit forms of modal parameters and the envelope of Green function of transient response for structures with a slightly detuned PTMD. Based on the perturbation techniques, he considered the PTMD detuning parameters directly and found that the envelope ratio of transient response has a smaller rate when the frequency difference between PTMD and main structure increases. Rana and Soong [20] assumed that the structural properties were known and examined the detuning effect on PTMD system parameters. They claimed that the detuning effect of the PTMD frequency ratio is more pronounced than that of the damping ratio. With the increase in structural damping ratio and the PTMD mass ratio, the detuning effect becomes less severe.

To solve the PTMD detuning effect, one of the promising methods is the application of multiple tuned mass dampers (MTMDs) with distributed masses and natural frequencies. Structural vibration control using MTMDs was first proposed by Clark [21] and then intensively studied by other researchers [22–24]. They showed that MTMDs had better control performance than single PTMD, particularly while the detuning effect exists. In most previous studies, a PTMD or MTMD was designed to control the fundamental modal vibration for a m.d.o.f. primary structure under wind or earthquake loading. Parametric studies in references [25–27] showed that while there were significant reductions in responses for the particular vibration mode being controlled, the higher modes may become the dominant modes of vibration for certain external excitations. In order to solve this problem, the application of several PTMDs tuned to different modes of the primary structure might require [20]. However, this would result in a modal contamination problem. PTMDs tuned to higher modes will deteriorate the first modal response reduction.

From the above discussions, it is clear that the PTMD control philosophy and the accurate estimation of primary structural parameters to reduce the detuning problem are two essential subjects. Unlike the previous studies, this paper investigated the change of the displacement and acceleration response spectra for structures with and without PTMD under various earthquake excitations. The overall PTMD effect on structural responses is clearly demonstrated. Moreover, it is generally recognized that the design of an optimal PTMD requires a prior knowledge of the modal parameters of the controlled structure to avoid the PTMD detuning effect. The vibration control verification of a PTMD is also needed through system identification after its implementation. Thus, it is important that system identification be carried out in conjunction with structural control. Traditional system identification techniques require the full measurement of excitation and its corresponding responses. However, the input excitation is generally difficult to define and measure accurately. Moreover, a real structure, such as a tall building, usually possesses a large number of degrees of freedom. It is impossible and impractical to acquire full

measurements because of the limited number of sensors. Thus, system identification based only on response measurements at a few degrees-of-freedom become necessary from a practical point of view. In this paper, the theoretical background to determine PTMD optimal parameters is introduced. The extended random decrement method combined with the Ibrahim time domain technique [28] is employed to identify the modal frequencies, damping ratio and mode shapes of a m.d.o.f. building-PTMD system based on a few floor response measurements. The difference in identified modal parameters between a structure with and without PTMDs indicates the vibration control effectiveness of PTMDs. Numerical results using a five-storey building-PTMD system show that the proposed system identification technique is favorable for actual implementation and that the PTMD is a useful control device.

2. OPTIMAL PASSIVE TUNED MASS DAMPERS

The concept of the PTMD dates back to 1909 [29]. Since then, much research has been carried out to examine its effectiveness for different dynamic load applications. The success of such a system in reducing wind-excited structural responses is now well established. However, because of the complex characteristics of earthquake excitations, there still has not been a general agreement on the effectiveness of PTMD systems to suppress seismic responses. In general, earthquake excitation is a random process whose frequency content, appearance, amplitude, and duration, etc., are all unpredictable. Most of the researchers assumed the excitation to be a white-noise random process in the design stage, and then verified the effectiveness of PTMD by applying real earthquake excitation. These case studies were limited to specified structures subjected to a single earthquake. No overall design philosophy of such a control device was investigated. Thus, general conclusions could not be drawn from the previous researches.

2.1. THE DESIGN PHILOSOPHY AND SEISMIC EFFECTIVENESS OF PTMD

Figure 2 shows the typical transfer function of the specified mode of a structure with and without PTMD which is designed based on the optimization procedure by Lin *et al.* [4]. It

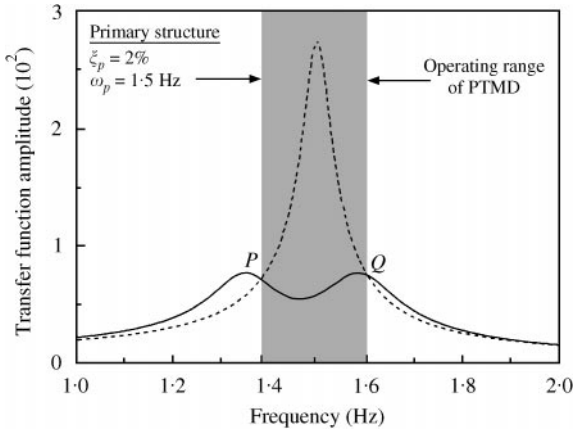

Figure 2. Typical transfer function of a structure with and without optimal PTMD: - - - - - - -, w/o PTMD; ——, with PTMD.

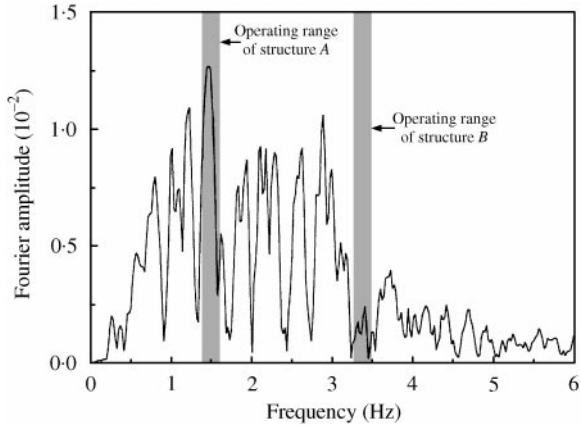

Figure 3. Fourier amplitude spectrum of 1995 Kobe earthquake and the operating range of PTMD for structures A and B.

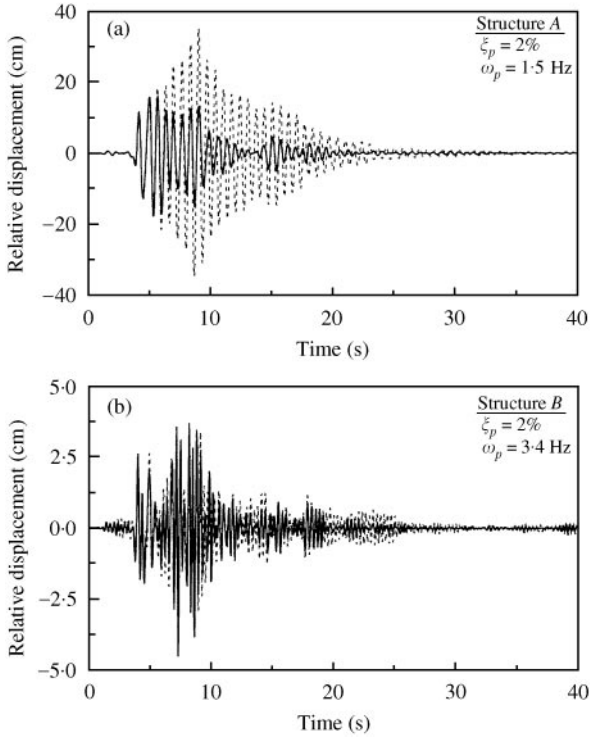

Figure 4. Relative displacement time history of structures A and B with and without PTMD under 1995 Kobe earthquake: - - - - - - -, w/o PTMD; ——, with PTMD.

is seen that these two curves intersect at points P and Q. It is known that the positions of P and Q vary with the PTMD's natural frequency, ω_s, and their elevations are independent of the PTMD's damping ratio, ξ_s. It is also seen that the transfer function of a structure with PTMD decreases in the frequencies between P and Q (operating range), but is unavailing and even amplifies in the other frequencies. Thus, it is expected that the PTMD will not produce vibration reduction unless the frequency content of an earthquake is within the

operating range. Otherwise, the PTMD will be ineffective. This phenomenon can be verified in the time domain using two s.d.o.f. structures A ($\omega_p = 1{\cdot}5$ Hz, $\xi_p = 2\%$) and B($\omega_p = 3{\cdot}4$ Hz, $\xi_p = 2\%$) subjected to the 1995 Kobe horizontal earthquake acceleration. Figure 3 shows the Fourier amplitude spectrum of the Kobe earthquake and the operating ranges of structures A and B. It is clearly seen that structure A falls in the major frequency-content range of the Kobe earthquake, whereas structure B does not. Their displacement time histories are illustrated in Figures 4(a) and 4(b) which show that the performance of PTMD is obviously excellent for structure A, but is not good for structure B, as expected in the frequency domain. This result implies that the seismic effectiveness of PTMD is highly frequency dependent. It operates efficiently only under resonant conditions. In previous research, PTMD was intuitively thought to be ineffective because of this phenomenon. However, although PTMD is less useful outside the resonant conditions, the structural response is small in this situation. Therefore, the PTMD is a useful control device in reducing the "excessive" seismic responses, which occurs during the resonant conditions.

In order to further understand the seismic effectiveness of PTMD, the relative displacement and absolute acceleration response spectra for s.d.o.f. structures ($\xi_p = 2\%$) with and without PTMD and PTMD under the 1985 Mexico and 1995 Kobe earthquakes,

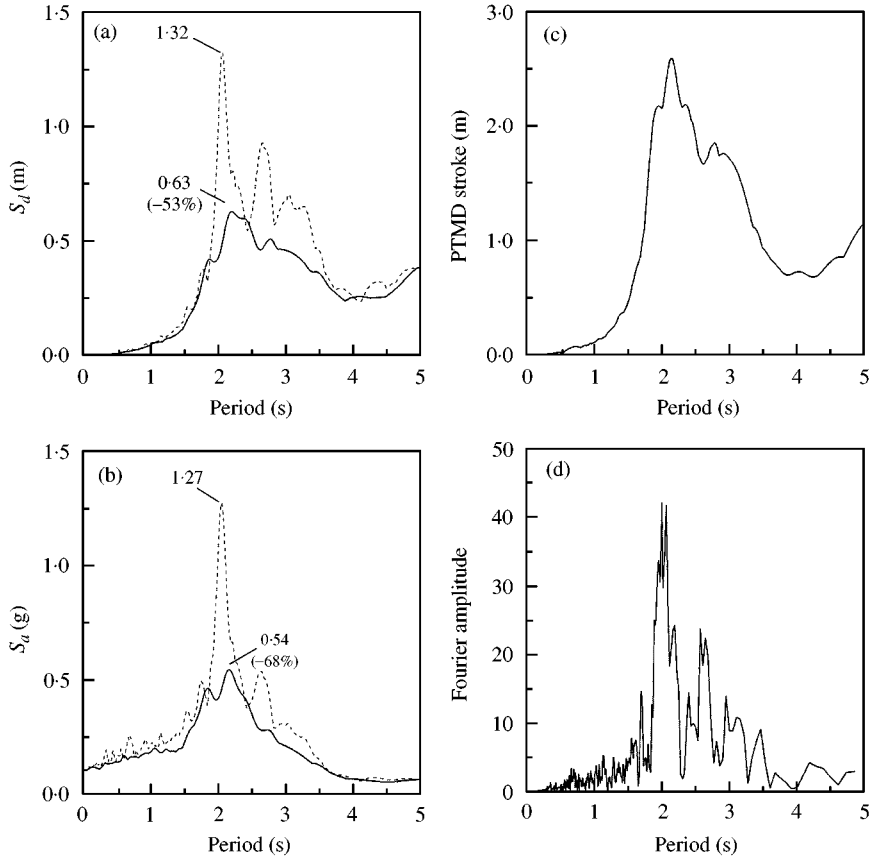

Figure 5. Response spectra of a structure ($\xi_p = 2\%$) with and without PTMD under 1995 Mexico earthquake: (a) displacement response spectrum; (b) acceleration response spectrum; (c) PTMD stroke and (d) Fourier amplitude spectrum of Mexico earthquake: - - - - - - -, w/o PTMD; ——, with PTMD.

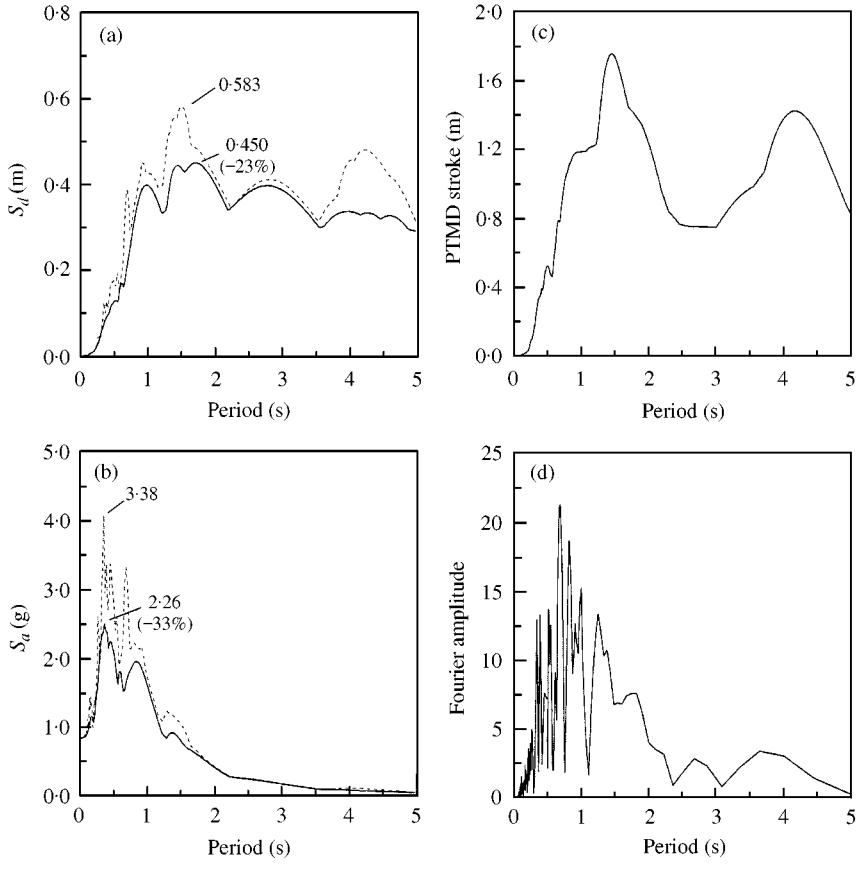

Figure 6. Response spectra of a structure ($\xi_p = 2\%$) with and without PTMD under 1995 Kobe earthquake: (a) displacement response spectrum; (b) acceleration response spectrum; (c) PTMD stroke and (d) Fourier amplitude spectrum of 1995 Kobe earthquake: - - - - - - -, w/o PTMD; ——, with PTMD.

are depicted in Figures 5 and 6. The dominant period ranges for each earthquake were less than 5 s, so were the maximal structural absolute acceleration and relative displacement responses. For structures with periods away from the dominant periods, no excessive responses will occur. Thus, PTMD application was not necessary. In Figures 5 and 6, it is seen that the maximum responses of structures with PTMD (solid line) are smaller than those without PTMD (dash line). Meanwhile, the maximal peak responses of structures with PTMD also occur near the same period for each case. As discussed earlier, the most effective cases for PTMD in reducing absolute acceleration (68% and 33% respectively) occurred under the worst resonant conditions. The PTMD strokes are also shown in Figures 5(c) and 6(c). It is clearly observed that the structural period, in which the maximal PTMD stroke occurs, was coincident with that of the optimum effectiveness of PTMD. To produce a comprehensive survey, after PTMD has been installed in a structure, the spectrum envelope for all cases is below those of the situations where the structure does not have PTMD. Although the peak responses are indeed amplified for structures with PTMD within some specified periods, these conditions are few and not always encountered at the worst situation. Meanwhile, the amount of amplification is limited. Therefore, they could not be used to conclude that PTMD is ineffective in a seismic application.

2.2. OPTIMAL PTMD SYSTEM PARAMETERS FOR MDOF BUILDING

The equations of motion for a s.d.o.f. PTMD mounted at the ith floor of an n-d.o.f. building structure under earthquake excitation, as show in Figure 1, can be written as

$$\mathbf{M}\ddot{\mathbf{x}}(t) + \mathbf{C}\dot{\mathbf{x}}(t) + \mathbf{K}\mathbf{x}(t) = -\mathbf{M}\mathbf{1}\ddot{x}_g(t), \tag{1}$$

in which

$$\mathbf{M} = \begin{bmatrix} \mathbf{M}_p & \mathbf{0} \\ \mathbf{0}^{\mathrm{T}} & m_s \end{bmatrix}, \quad \mathbf{C} = \begin{bmatrix} \mathbf{C}_p & \mathbf{0} \\ \mathbf{0}^{\mathrm{T}} & \mathbf{0} \end{bmatrix} + c_s \mathbf{u}\mathbf{u}^{\mathrm{T}}, \quad \mathbf{K} = \begin{bmatrix} \mathbf{K}_p & \mathbf{0} \\ \mathbf{0}^{\mathrm{T}} & 0 \end{bmatrix} + k_s \mathbf{u}\mathbf{u}^{\mathrm{T}}$$

are $(n+1)\times(n+1)$ mass, damping and stiffness matrices of the combined system. m_s, c_s, and k_s are the PTMD's mass, damping and stiffness. $\mathbf{x}(t) = [\mathbf{x}_p^{\mathrm{T}}(t), x_s(t)^{\mathrm{T}}]$ is the displacement vector. $\mathbf{x}_p(t)$ and $x_s(t)$ denote the displacements of primary structure and PTMD relative to the base. $\mathbf{1}$ is a vector with each element of 1. $\ddot{x}_g(t)$ represents the earthquake ground acceleration. Vector $\mathbf{u}^{\mathrm{T}} = [0, \ldots, 0, -1^{(i)}, 0, \ldots, 0, 1^{(n+1)}]$ indicates the location of the PTMD and the superscript T denotes the matrix transpose.

Define $v = (x_s - x_i)$, the PTMD displacement relative to the ith floor, as the PTMD's stroke. The equations of motion for the controlled structure and PTMD are given, respectively, as

$$\mathbf{M}_p\ddot{\mathbf{x}}_p(t) + \mathbf{C}_p\dot{\mathbf{x}}_p(t) + \mathbf{K}_p\mathbf{x}_p(t) = -\mathbf{M}\underline{\mathbf{1}}\ddot{x}_g(t) + \mathbf{f}_{\mathrm{TMD}}(t), \tag{2}$$

$$m_s(\ddot{v} + \ddot{x}_i) + c_s\,\dot{v} + k_s v = -m_s\ddot{x}_g. \tag{3}$$

In equation (2), the vector $\mathbf{f}_{\mathrm{TMD}} = [0, \ldots, 0, (c_s\dot{v} + k_s v), 0, \ldots, 0]^{\mathrm{T}}$ indicates the load of $(c_s\dot{v} + k_s v)$ acting on the ith floor of the structure by PTMD. Provided that the PTMD is tuned to the jth mode of the controlled structure and only the jth modal response is considered, the equations of motion for the jth mode and PTMD are expressed in the matrix form as

$$\begin{bmatrix} 1 & 0 \\ \phi_{ij} & 1 \end{bmatrix} \begin{Bmatrix} \ddot{\eta}_j \\ \ddot{v} \end{Bmatrix} + \begin{bmatrix} 2\xi_j\omega_j & -\mu_j(2\xi_s\omega_s) \\ 0 & 2\xi_s\omega_s \end{bmatrix} \begin{Bmatrix} \dot{\eta}_j \\ \dot{v} \end{Bmatrix} + \begin{bmatrix} \omega_j^2 & -\mu_j\omega_s^2 \\ 0 & \omega_s^2 \end{bmatrix} \begin{Bmatrix} \eta_j \\ v \end{Bmatrix} = -\begin{Bmatrix} \Gamma_j \\ 1 \end{Bmatrix} \ddot{x}_g, \tag{4}$$

where η_j, ξ_j and ω_j are the jth modal displacement, damping ratio and frequency of the controlled structure, ϕ_{ij} is the ith value of the jth mode shape, $\boldsymbol{\phi}_{ij}$; and $\omega_s = \sqrt{k_s/m_s}$ is the natural frequency of PTMD, $\xi_s = c_s/(2m_s\omega_s)$ is the damping ratio of PTMD, $\mu_j = \phi_{ij}(m_s/m_j^*)$ is the jth modal mass ratio, $m_j^* = \sum_{l=1}^{n}(\phi_{lj}^2 m_l)$ is the jth generalized modal mass of the controlled structure and $\Gamma_j = (\sum_{l=1}^{n}\phi_{lj}m_l)/m_j^*$ is the jth modal participation factor.

In the case of a s.d.o.f. structure with PTMD, $\phi_{ij} = \Gamma_j = 1$, μ_j represents the mass ratio of the PTMD to the structure and equation (4) is reduced to that of the conventional two-d.o.f. structure-PTMD system.

According to Lin *et al.* [4], the optimal PTMD's parameters are determined by minimizing the mean-square displacement response ratio of the first mode, $R_{dE,1}$, between the structure with and without the PTMD installation under earthquake excitation. The value of $R_{dE,1}$ smaller than unity represents the attenuation of the structural response due to

the presence of PTMDs. It is found [4] that PTMDs are more appropriate for a structure in which the fundamental frequency is less than that of the earthquake excitation, which is real for high-rise buildings or towers located on firm ground. In this case, the earthquake excitation can be simulated using white noise and $R_{dE,1}$ takes the form as

$$R_{dE,1} = \frac{E[\eta_1^2]_{\text{PTMD}}}{E[\eta_1^2]_{\text{NOPTMD}}} = \frac{\int_{-\infty}^{\infty} |H_{\eta_1 \ddot{x}_g}(\omega)|^2_{\text{PTMD}} S_{\ddot{x}_g}(\omega)\,\mathrm{d}\omega}{\int_{-\infty}^{\infty} |H_{\eta_1 \ddot{x}_g}(\omega)|^2_{\text{NOPTMD}} S_{\ddot{x}_g}(\omega)\,\mathrm{d}\omega} = \frac{A}{B}, \tag{5}$$

in which $S_{\ddot{x}_g}(\omega) = S_0$ represents constant ground intensity and

$$\begin{aligned} A = {} & 4\xi_1\xi_s^2 r_f^3(\Gamma_1 + \mu_1)^2(1 + \phi_{i1}\mu_1) + 4\xi_1^2\xi_s^3 r_f^4(\Gamma_1 + \mu_1)^2(1 + \phi_{i1}\mu_1) \\ & + 4\xi_1^2\xi_s^2 r_f^2(\Gamma_1 + \mu_1)^2 + 4\xi_1^3\xi_s r_f^3(\Gamma_1 + \mu_1)^2 - \xi_1\xi_s r_f^3(\Gamma_1^2 - \mu_1^2)(1 + \phi_{i1}\mu_1) \\ & - \xi_1\xi_s r_f^3(\Gamma_1 + \mu_1)^2 + \xi_1\xi_s r_f^5(\Gamma_1 + \mu_1)^2(1 + \phi_{i1}\mu_1)^2 + \Gamma_1^2\xi_1\xi_s r_f + \xi_1^2 r_f^2\mu_1^2 \\ & + \xi_1^2 r_f^4(\Gamma_1 + \mu_1)^2\phi_{i1}\mu_1, \\ B = {} & 4\Gamma_1^2\xi_1\xi_s^3 r_f^3(1 + \phi_{i1}\mu_1) + 4\Gamma_1^2\xi_1^2\xi_s^2 r_f^2 + \Gamma_1^2\xi_s^2 r_f^2\phi_{i1}\mu_1 + 4\Gamma_1^2\xi_1^2\xi_s^2 r_f^4(1 + \phi_{i1}\mu_1) \\ & + \Gamma_1^2\xi_1\xi_s r_f + 4\Gamma_1^2\xi_1^3\xi_s r_f^3 - 2\Gamma_1^2\xi_1\xi_s r_f^3 + \Gamma_1^2\xi_1\xi_s r_f^5(1 + \phi_{i1}\mu_1) + \Gamma_1^2\xi_s^2 r_f^4\phi_{i1}\mu_1. \end{aligned}$$

In equation (5), $r_f = \omega_s/\omega_1$ is defined as the ratio of PTMD's frequency to the fundamental frequency of the controlled structure. It is seen that $R_{dE,1}$ is a function of ξ_1, ϕ_{i1} (structural parameters); μ_1, ξ_s, and r_f (PTMD's parameters) and is independent of ω_1. For the given values of ξ_i and ϕ_{i1}, the optimal PTMD's design parameters can be obtained by differentiating $R_{dE,1}$ with respect to r_f, ξ_s and μ_1, and equating to zero, respectively, to minimize $R_{dE,1}$. Their values may be found by solving the following equations simultaneously:

$$\frac{\partial R_{dE,1}}{\partial \xi_s} = 0, \quad \frac{\partial R_{dE,1}}{\partial r_f} = 0, \quad \frac{\partial R_{dE,1}}{\partial \mu_1} = 0. \tag{6}$$

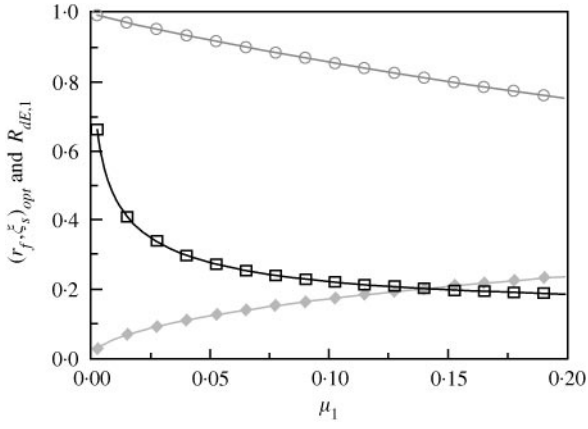

Figure 7. Optimal r_f, ξ_s and $R_{dE,1}$ for five-storey uniform shear building with $\xi_1 = 2\%$: —○—, r_f; —◆—, ξ_s; —□—, $R_{dE,1}$.

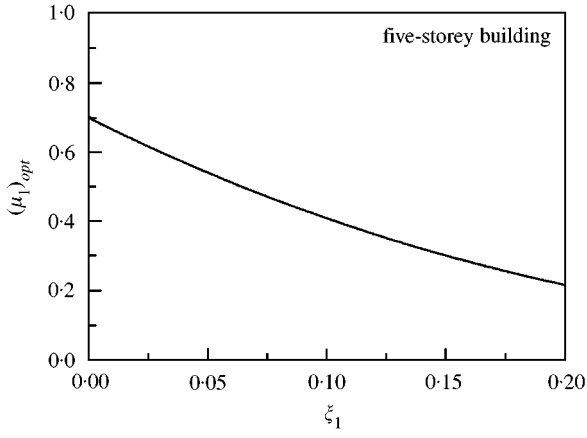

Figure 8. Optimal modal mass ratio for five-storey uniform shear building with various ξ_1.

In practice, $(\mu_1)_{opt}$ is rarely used due to economic considerations. Hence, we may first find out $(\xi_s)_{opt}$ and $(r_f)_{opt}$ for various values of ξ_1 and μ_1, and then search for $(\mu_1)_{opt}$. For a uniform five-storey shear building with equal mass and stiffness at each floor and a PTMD installed at the top floor, the optimal values of ξ_s, r_f and their corresponding $R_{dE,1}$ for various values of ξ_1 and μ_1 are illustrated in Figure 7. It is found that r_f decreases as μ_1 and ξ_1 increase. ξ_s increases gradually as μ_1 increases but is generally independent on ξ_1, and $R_{dE,1}$ decreases significantly as μ_1 increases. Moreover, an optimal μ_1 exists to make $R_{dE,1}$ minimum. It is a function of ξ_1 and ϕ_{i1} and decreases as ξ_1 increases, as seen in Figure 8. It has been shown that with the installation of optimal PTMDs, the equivalent first modal damping ratio is always greater than the original damping ratio.

2.3. THE INFLUENCE OF SITE EFFECT ON PTMD'S OPTIMAL PARAMETERS

In the previous section, the earthquake excitation is regarded as a white noise in the evaluation of PTMD's optimal parameters. Such obtained parameters may not be really optimal because the excitation frequency dependency is not taken into account. In the real situation, the soil properties of a specified site will significantly alter the dynamic properties of the excitations generated from any source. To include the site effect, the earthquake excitation is generally modelled as the Kanai–Tajimi spectrum and takes the form as

$$S_{\ddot{x}_g}(\omega) = \frac{4\xi_g^2\omega_g^2\omega^2 + \omega_g^4}{(\omega_g^2 - \omega^2)^2 + 4\xi_g^2\omega_g^2\omega^2} S_0, \tag{7}$$

where ω_g and ξ_g represent the dominant frequency and damping ratio of the site respectively. Again, considering the five-storey uniform shear building installed with a PTMD of $\mu_1 = 5\%$, the PTMD's optimal ξ_s and r_f and the mean-squared response ratio, $R_{dE,1}$ are shown in Figure 9 (solid lines) for various excitation to structure frequency ratios, ω_g/ω_1, and compared with those determined from white noise excitation (dash lines). It is clearly seen that the site effect can be ignored as ω_g/ω_1 is greater than 1·0 for primary structures built on hard site. On the other hand, the PTMD's optimal parameters slightly change as ω_g/ω_1 is less than 1·0, especially for r_f. This is due to the fact that the dominant

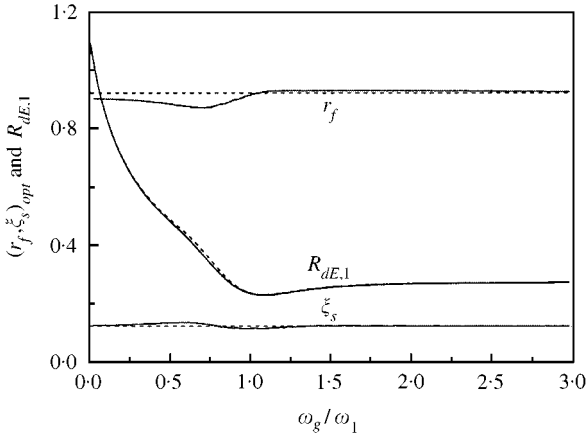

Figure 9. Optimal r_f, ξ_s and $R_{dE,1}$ for five-storey uniform shear building with PTMD designed by white noise or Kanai–Tajimi spectrum ($\xi_g = 32\%$): ---------, white noise; ———, Kanai–Tajimi spectrum.

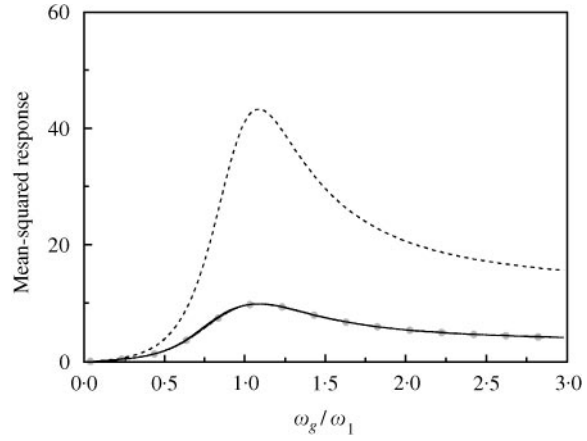

Figure 10. Mean-square responses of five-storey uniform shear building without and with PTMD ($\xi_g = 32\%$): ---------, without PTMD; ---●---, with PTMD (designed by Kanai–Tajimi); ———, with PTMD (designed by white noise).

frequency of excitations tends to excite the left resonant peak of the structure-PTMD system, which is out of the operating range as shown in Figure 2. Hence, the PTMD's optimization criterion lowers r_f to reduce the value of left peak (point P in Figure 2) to avoid significant amplification. However, this will cause the amplification of right peak (point Q in Figure 2) as r_f becomes small. To take a balance between two peaks and their corresponding frequency contents of the excitation and to maintain the tuning condition of PTMD to primary structure, the change of r_f will be limited within a small range. However, it is noted that the mean-squared response ratios, $R_{dE,1}$, by using the PTMD's optimal parameters designed with and without the consideration of the site effect are nearly identical. Furthermore, since the site effect for earthquake excitation is uncertain and is not easy to predict accurately, it is recommended that the PTMD's optimal parameters be evaluated using the procedure mentioned in the previous section. A phenomenon is also observed that when ω_g/ω_l is smaller than 0·5, $R_{dE,1}$ is large. It seems that the PTMD is not useful. Actually, for those situations, the mean-squared structural responses are really small, as shown in Figure 10. Any vibration control device is not necessary.

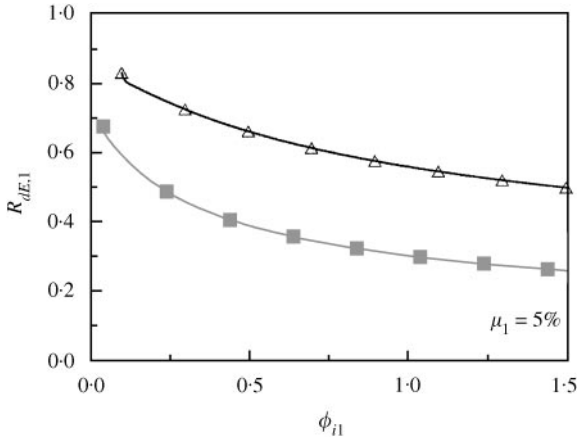

Figure 11. $R_{dE,1}$ varies with ξ_1 and ϕ_{i1} for uniform shear building: ---■---, $\xi_1 = 2\%$; —△—, $\xi_1 = 5\%$.

2.4. OPTIMAL PTMD LOCATION

As mentioned above, most of the previous researches assumed the controlled structure as a s.d.o.f. system with fundamental modal properties. No optimum location for PTMD was investigated. According to equation (5), we know that $R_{dE,1}$ depends on ϕ_{i1}, the mode shape value of the floor on which the PTMD is installed. This implies that an optimum PTMD location may exist such that $R_{dE,1}$ has a minimum given value for each ξ_1 and μ_1. Figure 11 illustrates the relationship between $R_{dE,1}$ and the two parameters of ξ_1 and ϕ_{i1} for $\mu_1 = 5\%$. It is shown that $R_{dE,1}$ decreases as ϕ_{i1} increases for any specified damping ratio ξ_1. Thus, the position with the largest value in the controlled mode shape is the optimum location for the PTMD.

It is noted that the determination of the optimum location described above was investigated in the modal space. In order to demonstrate this finding in a more physical way, a PTMD with mass ratio to the total mass of primary structure, $\mu = 2{\cdot}85\%$, for a five-storey building, whose properties are given in Table 1, was examined. The optimization procedure was performed as the PTMD was placed at different floors. The sets of optimal frequency ratio and damping ratio $(r_f, \xi_s)_{opt}$ and increment of first modal damping ratio [4] are calculated and illustrated in Figure 12. It is clearly seen that the higher the PTMD is located, the greater the damping ratio and less the PTMD stiffness are required and greater the modal damping ratio is obtained. The installation of PTMD at the fifth floor results in an additional first modal-damping ratio of 5·49%. The R_{dE} and R_{aE} of each floor when PTMD ($\mu = 2{\cdot}85\%$) is installed at different floors is depicted in Figure 13. As expected, both R_{dE} and R_{aE} are minimum when PTMD is located on the fifth floor (i.e., the top floor) where the first mode shape value is the largest compared with that of the other floors. The reduction in upper floor responses is larger than the responses for the lower floors. This proves the vibration control effectiveness of PTMDs.

3. MODAL PARAMETER IDENTIFICATION

As seen in the preceding sections, to determine the PTMD's optimal parameters requires a prior knowledge of ω_1, ξ_1 and ϕ_1. For a controlled structure with unknown parameters, a system identification technique should be used to identify these parameters. In this study,

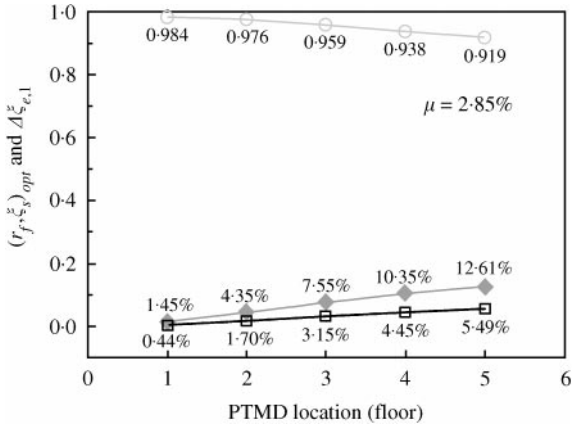

Figure 12. Optimal-damping and -frequency ratios for PTMD installed at different floor of five-storey building, and the corresponding increment of equivalent first modal-damping ratio: —○—, r_f; —◆—, ξ_s; —□—, $\Delta\xi_{e,1}$.

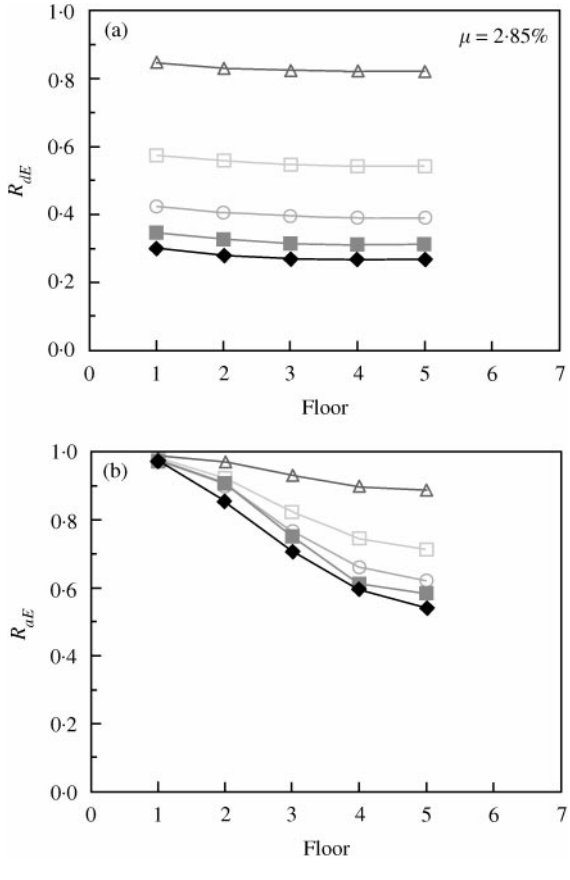

Figure 13. R_{dE} and R_{aE} of each floor when PTMD is installed at different floors of five-storey building ($\mu = 2{\cdot}85\%$): —◆—, 5F; - - -■- - -, 4F; - - -○- - -, 3F; - - -□- - -, 2F; —△—, 1F.

the extended random decrement method was employed first to extract the free vibration responses at measured locations. Then, the Ibrahim time domain technique was applied to calculate the structural modal frequencies, damping ratios, and mode shapes. The proposed

methods have great advantages when only response data, not the input excitation, are available.

3.1. EXTENDED RANDOM DECREMENT METHOD

Let $u(t)$ be a response measurement (with or without noise) at a certain location in a structure, as shown in Figure 14(a), induced by zero-mean, stationary random excitations. This time history is divided into short segments with duration t_d, which is several times the structural fundamental period. The random decrement method consists of the following steps of analysis to obtain a free decay response: (1) calculate an amplitude u_s, which is usually the root-mean-square value of $u(t)$; (2) select the starting time t_i for each segment such that

$$u(t_i) = u_s \quad i = 1, 2, 3, \ldots,$$

$$u(t_i) \geqslant 0 \quad i = 1, 3, 5, \ldots,$$

$$u(t_i) \leqslant 0 \quad i = 2, 4, 6, \ldots,$$

(3) average N_s segments of the response measurement to yield a time function, $\delta(\tau)$, i.e.,

$$\delta(\tau) = \frac{1}{N_s} \sum_{i=1}^{N_s} u(t_i + \tau), \quad 0 < \tau < t_d \tag{8}$$

called random decrement signature as shown in Figure 14(b).

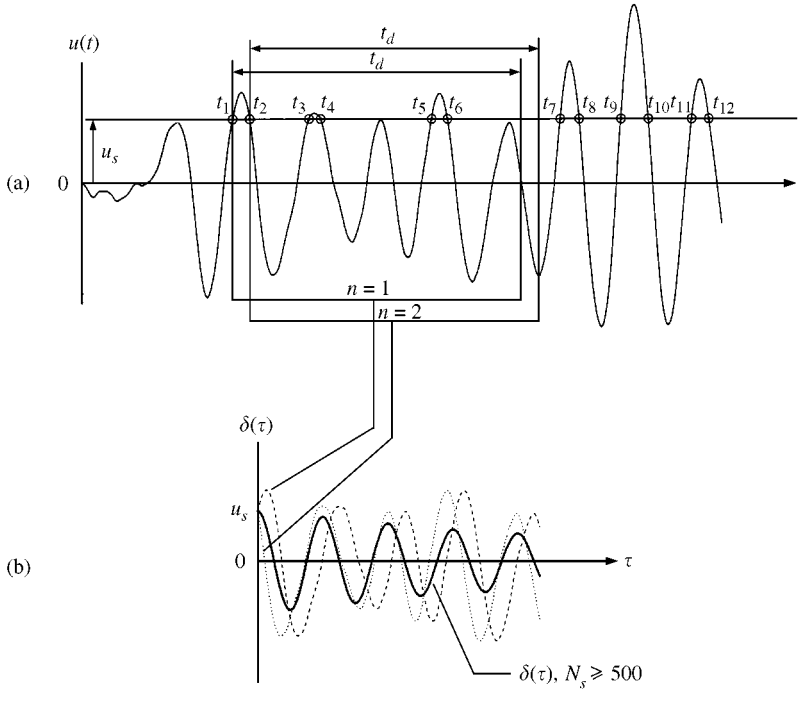

Figure 14. (a) Response measurement and crossing times; (b) Extraction of free decay signature from response measurement.

For a linear structure, its dynamic response can be decomposed into three parts including response due to the initial displacement, initial velocity, and external loading respectively. Following step (2) of the random decrement analysis procedure, the response due to initial velocity cancels out because parts with positive and negative initial slopes are random. In addition, since the external excitation is assumed to be a stationary random process with zero mean, the response due to external loading also vanishes. Hence, $\delta(\tau)$ represents a free decay response due to initial displacement. Furthermore, the unique form of random decrement signature and the lack of requirement to input excitation measurements make the random decrement method very attractive to use for system parameter identification and damage detection.

Basically, the original random decrement method was developed to process a single measurement. For multiple measurements taken from a real building, their correlations will be lost if the above analysis procedure is applied to each individual measurement independently. To overcome this problem, in this study, the crossing times t_i in step (2) were determined from one designated measurement. All measurements were then processed following step (3), simultaneously, to obtain their respective free decay signatures. For building structures, it is suggested that the lower floor measurement be used to determine the crossing times because it contains greater weight for the higher modes. Therefore, we can get enough number of segments to superimpose in equation (8) in a shorter record length. This proposal was proved successful in the following numerical example.

3.2. IBRAHIM TIME DOMAIN TECHNIQUE

The free decay response at measured station l and time t_j obtained from equation (8) can be expressed as the summation of m structural modes as

$$\delta_l(t_j) = x_{l,j} = \sum_{k=1}^{2m} \varphi_{lk} e^{\lambda_k t_j}, \tag{9}$$

where λ_k and φ_{lk} represent the kth complex eigenvalue and mode shape value at location l respectively. The modal frequency ω_k and damping ratio ξ_k are then calculated using

$$\omega_k = |\lambda_k|, \quad \xi_k = -\frac{\mathrm{Re}(\lambda_k)}{\omega_k}. \tag{10}$$

In equation (10), $\mathrm{Re}(\lambda_k)$ denotes the real part of λ_k. Suppose that the responses at n different stations are measured and m modal properties are to be identified, we may use any m measurements for s instants (when $n \geqslant m$) or repeat the available measurements (when $n < m$) to construct the response matrix $\mathbf{X}$ using time shifting schemes [30] such that

$$\mathbf{X} = \mathbf{\Psi}\mathbf{\Lambda}, \tag{11}$$

where

$$\mathbf{X} = \begin{bmatrix} x_{1,1} & x_{1,2} & \cdot & \cdot & x_{1,s} \\ x_{2,1} & x_{2,2} & \cdot & \cdot & x_{2,s} \\ \cdot & \cdot & \cdot & \cdot & \cdot \\ \cdot & \cdot & \cdot & \cdot & \cdot \\ x_{2m,1} & x_{2m,2} & \cdot & \cdot & x_{2m,s} \end{bmatrix}, \quad \mathbf{\Psi} = \begin{bmatrix} \varphi_{1,1} & \varphi_{1,2} & \cdot & \cdot & \varphi_{1,2m} \\ \varphi_{2,1} & \varphi_{2,2} & \cdot & \cdot & \varphi_{2,2m} \\ \cdot & \cdot & \cdot & \cdot & \cdot \\ \cdot & \cdot & \cdot & \cdot & \cdot \\ \varphi_{2m,1} & \varphi_{2m,2} & \cdot & \cdot & \varphi_{2m,2m} \end{bmatrix}, \tag{12a, 12b}$$

$$\mathbf{\Lambda} = \begin{bmatrix} e^{\lambda_1 t_1} & e^{\lambda_1 t_2} & \cdot & \cdot & e^{\lambda_1 t_s} \\ e^{\lambda_2 t_1} & e^{\lambda_2 t_2} & \cdot & \cdot & e^{\lambda_2 t_s} \\ \cdot & \cdot & \cdot & \cdot & \cdot \\ \cdot & \cdot & \cdot & \cdot & \cdot \\ e^{\lambda_{2m} t_1} & e^{2mt_2} & \cdot & \cdot & e^{\lambda_{2m} t_s} \end{bmatrix}. \tag{12c}$$

Similarly, the response matrix $\hat{\mathbf{X}}$ corresponding to the same measured stations and Δt later in time than those in equation (11) can be expressed as

$$\hat{\mathbf{X}} = \hat{\mathbf{\Psi}}\mathbf{\Lambda}. \tag{13}$$

In equation (13), the entries of matrices $\hat{\mathbf{X}}$ and $\hat{\mathbf{\Psi}}$ are related using

$$\hat{x}_{l,j} = \sum_{k=1}^{2m} \hat{\varphi}_{lk} e^{\lambda_k t_j}, \quad \hat{\varphi}_{lk} = \varphi_{lk} e^{\lambda_k \Delta t}. \tag{14}$$

The elimination of $\mathbf{\Lambda}$ from equations (11) and (13) gives

$$\hat{\mathbf{X}} = \hat{\mathbf{\Psi}}\mathbf{\Psi}^{-1}\mathbf{X} = \mathbf{A}\mathbf{X} \tag{15}$$

and

$$\mathbf{A}\mathbf{\Psi} = \mathbf{\Psi}\boldsymbol{\alpha}, \tag{16}$$

where $\mathbf{A}$ is defined as the $(2m \times 2m)$ system matrix. Equation (15) is generally an over-determined system of simultaneous linear equations. The solution to obtain matrix $\mathbf{A}$ is not unique. Several approaches such as the least-square method and singular value decomposition can be used. Moreover, equation (16) is a standard eigenvalue equation which can be solved using any conventional method. The matrix $\boldsymbol{\alpha}$ is a diagonal matrix with entries $\alpha_k = e^{\lambda_k \Delta t}$. Let $\alpha_k = \beta_k + i\gamma_k$ and $\lambda_k = a_k + ib_k$, $(i = \sqrt{-1})$, then a_k and b_k are related to β_k and γ_k as

$$a_k = \frac{1}{2\Delta t} \ln(\beta_k^2 + \gamma_k^2), \tag{17}$$

$$b_k = \frac{1}{\Delta t} \tan^{-1}\left(\frac{\gamma_k}{\beta_k}\right). \tag{18}$$

Once the eigenvalue λ_k is obtained, the kth modal frequency and damping ratio are calculated from equation (10). Based on the above derivations, it is also found that the eigenvectors $\mathbf{\Psi}$ of matrix $\mathbf{A}$ are the desired complex mode shapes of the structure.

3.3. MODE-SHAPE INTERPOLATION

Based on the Ibrahim time domain technique, all desired modal frequencies and damping ratios are found using equations (10), (14)–(16). Because of partial response measurements, only the mode shape values at the instrumental d.o.f.s can be identified. To obtain the

TABLE 1

Physical and modal parameters of five-storey building

Mass matrix, $\mathbf{M}$ ($\mathrm{N\,s^2/cm}$)

$$\begin{bmatrix} 19{\cdot}57 & 0 & 0 & 0 & 0 \\ 0 & 19{\cdot}57 & 0 & 0 & 0 \\ 0 & 0 & 19{\cdot}57 & 0 & 0 \\ 0 & 0 & 0 & 19{\cdot}57 & 0 \\ 0 & 0 & 0 & 0 & 19{\cdot}57 \end{bmatrix}$$

Damping matrix, $\mathbf{C}$ ($\mathrm{N\,s/cm}$)

$$\begin{bmatrix} 47{\cdot}19 & -13{\cdot}67 & -0{\cdot}79 & 0{\cdot}30 & 0{\cdot}06 \\ & 37{\cdot}46 & -15{\cdot}61 & -1{\cdot}04 & 0{\cdot}46 \\ & & 36{\cdot}22 & -16{\cdot}46 & 0{\cdot}11 \\ & \textit{sym.} & & 34{\cdot}26 & -14{\cdot}28 \\ & & & & 15{\cdot}93 \end{bmatrix}$$

Stiffness matrix, $\mathbf{K}$ ($\mathrm{N/cm}$)

$$\begin{bmatrix} 77108 & -36564 & 4549 & 1612 & -211 \\ & 58596 & -35825 & 5481 & 1169 \\ & & 58344 & -36587 & 7463 \\ & \textit{sym.} & & 52688 & -22962 \\ & & & & 14621 \end{bmatrix}$$

Modal natural frequencies, ω_j (Hz)

$$\begin{bmatrix} 0{\cdot}91 \\ 3{\cdot}37 \\ 7{\cdot}11 \\ 10{\cdot}66 \\ 12{\cdot}73 \end{bmatrix}$$

Modal damping ratio, ξ_j (%)

$$\begin{bmatrix} 2{\cdot}00 \\ 2{\cdot}00 \\ 2{\cdot}00 \\ 2{\cdot}00 \\ 2{\cdot}00 \end{bmatrix}$$

Mode shape matrix, $\mathbf{\Phi}$

$$\begin{bmatrix} 1{\cdot}00 & 1{\cdot}00 & 1{\cdot}00 & 1{\cdot}00 & 1{\cdot}00 \\ 3{\cdot}02 & 2{\cdot}12 & 0{\cdot}92 & -0{\cdot}33 & -1{\cdot}21 \\ 5{\cdot}27 & 1{\cdot}89 & -0{\cdot}64 & -0{\cdot}63 & 1{\cdot}12 \\ 7{\cdot}31 & 0{\cdot}18 & -0{\cdot}96 & 0{\cdot}88 & -0{\cdot}70 \\ 8{\cdot}96 & -2{\cdot}09 & 0{\cdot}74 & -0{\cdot}35 & 0{\cdot}21 \end{bmatrix}$$

complete mode shapes, we developed an interpolation method to calculate the mode shape values for the locations without measurement. It was assumed that the building mode shapes are linearly superimposed by the shear modes, $\varphi_i(j = 1, \ldots, n)$, of a corresponding building with the same mass distribution and uniform stiffness. Then, we can form a set of

functions $(\varphi_1 - \varphi_2)$, $(\varphi_1 - \varphi_3)$, $(\varphi_1 - \varphi_4)$, etc., as basic ingredients for mode shape interpolation. For instance, if three-floor translations are measured, the first three mode shapes are expressed as

$$\boldsymbol{\phi}_1 = \boldsymbol{\varphi}_1 + a_{11}(\boldsymbol{\varphi}_1 - \boldsymbol{\varphi}_2) + a_{12}(\boldsymbol{\varphi}_1 - \boldsymbol{\varphi}_3) \tag{19a}$$

$$\boldsymbol{\phi}_2 = \boldsymbol{\varphi}_2 + a_{21}(\boldsymbol{\varphi}_1 - \boldsymbol{\varphi}_2) + a_{22}(\boldsymbol{\varphi}_1 - \boldsymbol{\varphi}_3) + a_{23}(\boldsymbol{\varphi}_1 - \boldsymbol{\varphi}_4) \tag{19b}$$

$$\boldsymbol{\phi}_3 = \boldsymbol{\varphi}_3 + a_{31}(\boldsymbol{\varphi}_1 - \boldsymbol{\varphi}_2) + a_{32}(\boldsymbol{\varphi}_1 - \boldsymbol{\varphi}_3) + a_{33}(\boldsymbol{\varphi}_1 - \boldsymbol{\varphi}_4) + a_{34}(\boldsymbol{\varphi}_1 - \boldsymbol{\varphi}_5) \tag{19c}$$

where $a_{11}, a_{12}, \ldots$, are constant coefficients to be determined using the identified mode shape values and orthogonality conditions between modes. For a high-rise building, it is suggested that at least three sensors be installed at low, medium and top floors. The more floors that are instrumented, the more accurate the mode shapes obtained.

4. NUMERICAL VERIFICATIONS

A five-storey ($n = 5$) building with an optimal PTMD at the top floor is presented to verify the efficiency of the proposed identification methods and the vibration control effectiveness of the PTMDs. The structural and PTMD system parameters determined using equation (6) are given in Tables 1 and 2. Structural damping of 2% is assumed for all modes. First of all, we pretended that the structural properties were unknown. Full or partial (1F, 3F, and 5F) floors were instrumented to measure their translations due to random ambient vibrations. Two cases with noise-free and noise-to-signal ratio (NSR) equal to 20% were studied to investigate the influence of the measurement noise level. First, the extended random decrement method was performed to extract the free vibration, also called the random decrement signatures of floors from the measurements. In the case of NSR = 20%, the relative displacement measurements and random decrement signatures for all floors are illustrated in Figure 15. Then, based on the extracted signatures, the Ibrahim time domain method was used to identify the modal properties of the system. Table 3 shows the identified structural frequencies and damping ratios, whereas Figure 16 depicts the mode shapes based on the proposed identification methods and mode shape interpolation scheme. For full measurement without noise, the identified parameters should be very close to the true parameters. The estimation error increases for partial measurements as well as high noise levels. The identification accuracy of the damping ratio is not as good as that for modal frequency and mode shape, but is still adequate for accurate PTMD parameter design because ξ_s and r_f are not sensitive to the variation of structural modal dampings.

TABLE 2

Physical and modal parameters of PTMD

Modal parameters	Modal mass ratio, μ_1 (mass ratio, μ)	5% (2·85%)
	Frequency ratio, r_f	0·92
	Damping ratio, ξ_s	12·6%
Physical parameters	Mass, m_s(Ns^2/m)	2·79
	Damping coefficient, c_s (Ns/m)	77·8
	Stiffness coefficient, k_s (N/m)	3·72

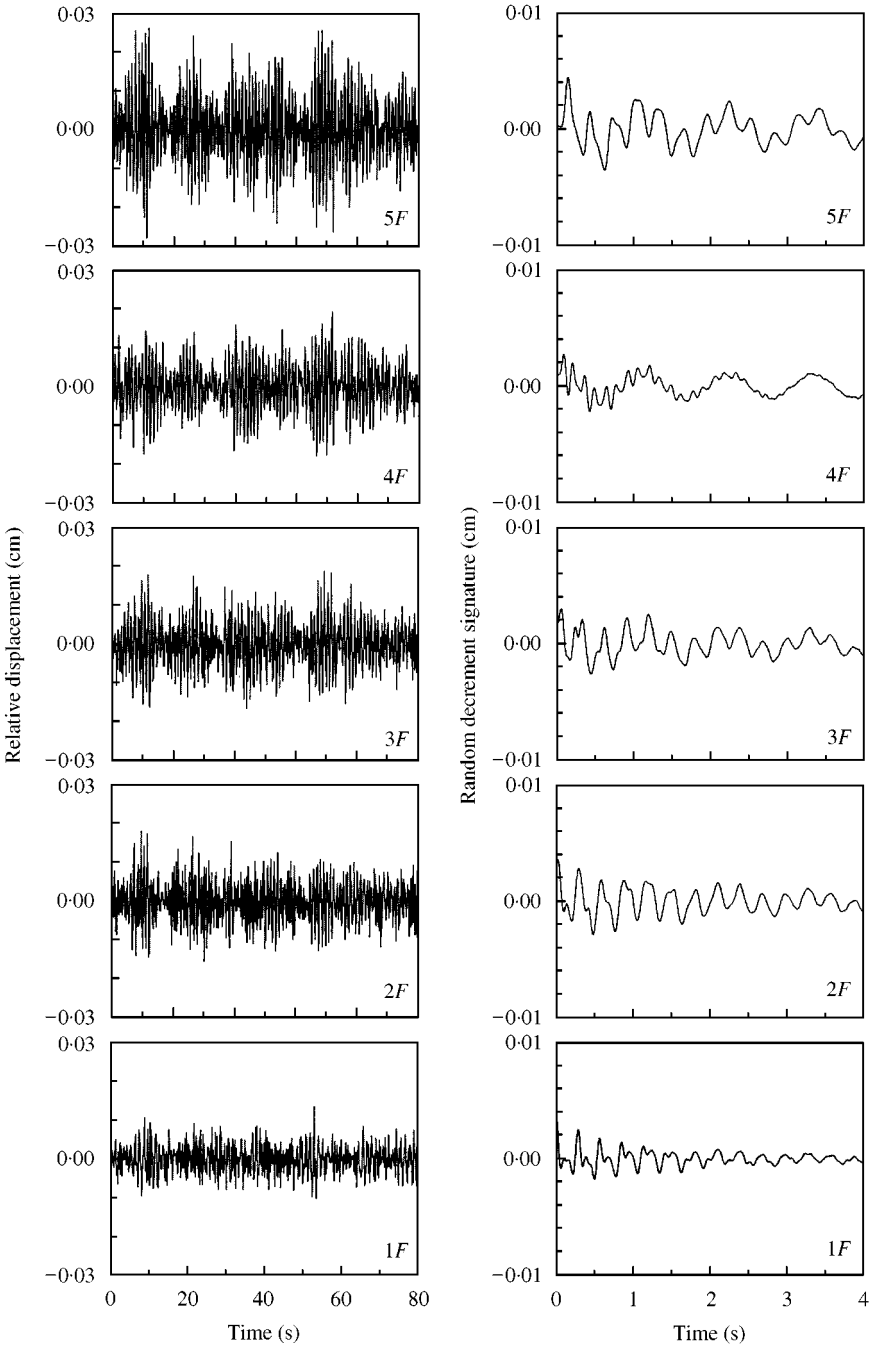

Figure 15. Response measurements and random decrement signature of five-storey building (NSR = 20%).

In addition, the modal frequencies, damping ratios, and the first four mode shapes of the five-storey building-PTMD system, whose full ambient vibration measurements and random decrement signatures for the case of NSR = 20%, shown in Figure 17, are also identified and presented in Table 4 and Figure 18. It is seen that for partial measurements

TABLE 3

Identified modal frequencies and damping ratios for a five-storey building

	Natural frequency (Hz)					Damping ratio (%)				
		NSR = 0%		NSR = 20%			NSR = 0%		NSR = 20%	
Mode	True	Full	Partial	Full	Partial	True	Full	Partial	Full	Partial
1	0·915	0·910 (− 0·6%)	0·912 (− 0·3%)	0·901 (− 1·5)	0·898 (− 1·9%)	2·000	2·166 (+ 8%)	1·685 (− 16%)	1·607 (− 21%)	1·647 (− 18%)
2	3·371	3·360 (− 0·3%)	3·356 (− 0·4%)	3·360 (− 0·3%)	3·358 (− 0·4%)	2·000	1·556 (− 22%)	1·637 (− 18%)	1·569 (− 22%)	1·662 (− 17%)
3	7·107	7·138 (+ 0·4%)	7·124 (+ 0·2%)	7·143 (+ 0·5%)	7·130 (+ 0·3%)	2·000	1·448 (− 28%)	1·481 (− 26%)	1·509 (− 25%)	1·464 (− 27%)
4	10·657	10·616 (− 0·4%)	10·621 (− 0·3%)	10·627 (− 0·3%)	10·647 (− 0·1%)	2·000	2·278 (+ 14%)	2·106 (+ 5%)	1·940 (− 3%)	1·947 (− 3%)
5	12·728	12·292 (− 3·4%)	12·281 (− 3·5%)	12·240 (− 3·8%)	12·087 (− 5·0%)	2·000	2·190 (+ 10%)	2·024 (+ 1%)	2·233 (+ 12%)	2·036 (+ 2%)

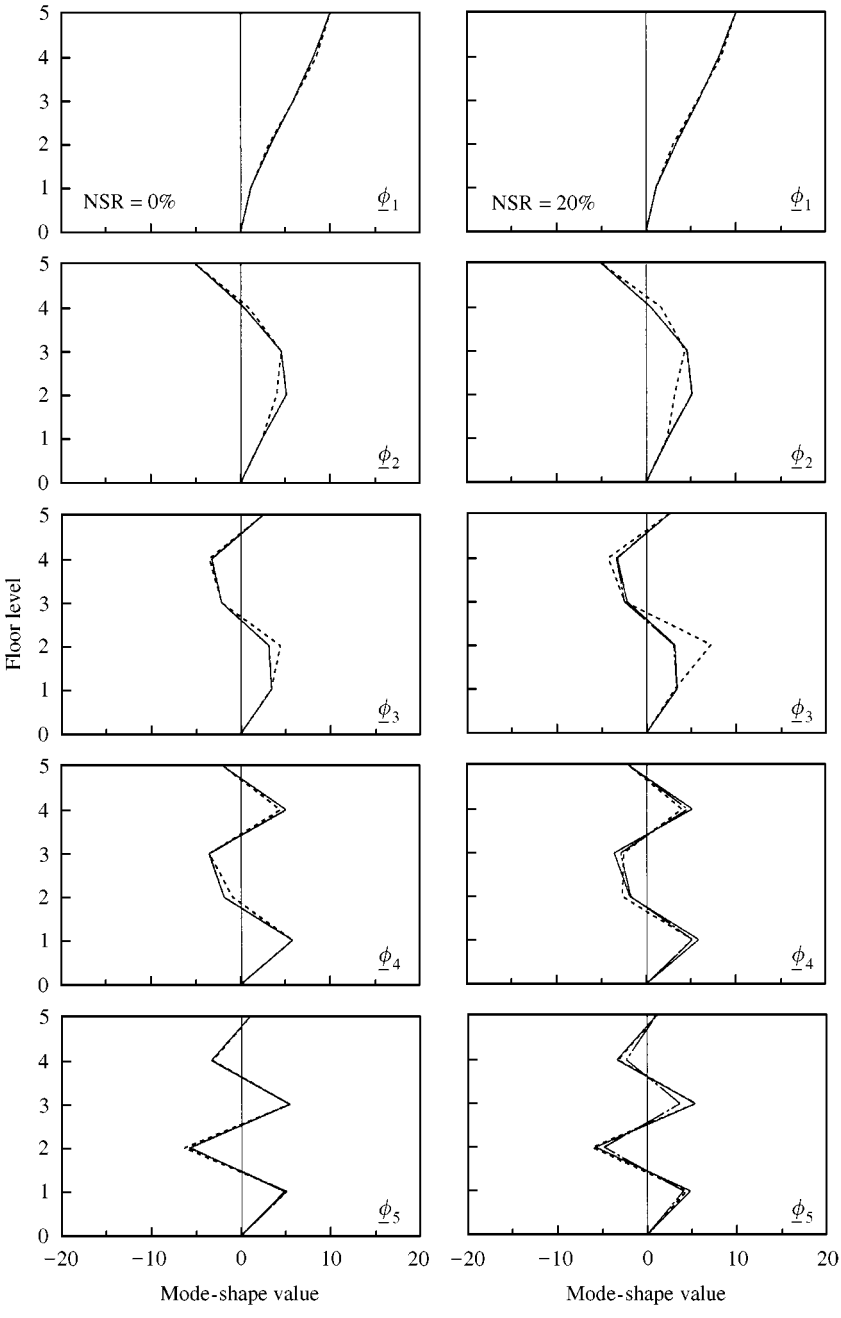

Figure 16. Calculated versus true mode shapes of five-storey building: ———, true; —·—, full measurements; - - - - - - - - -, 1, 3, 5F measurements.

with NSR = 20%, the proposed method is still able to identify most of the dominant modal parameters accurately even with very close modes (the first and second modes). These identification results are generally adequate for structural response prediction and PTMD performance evaluation because the total responses are dominated by the first few modes.

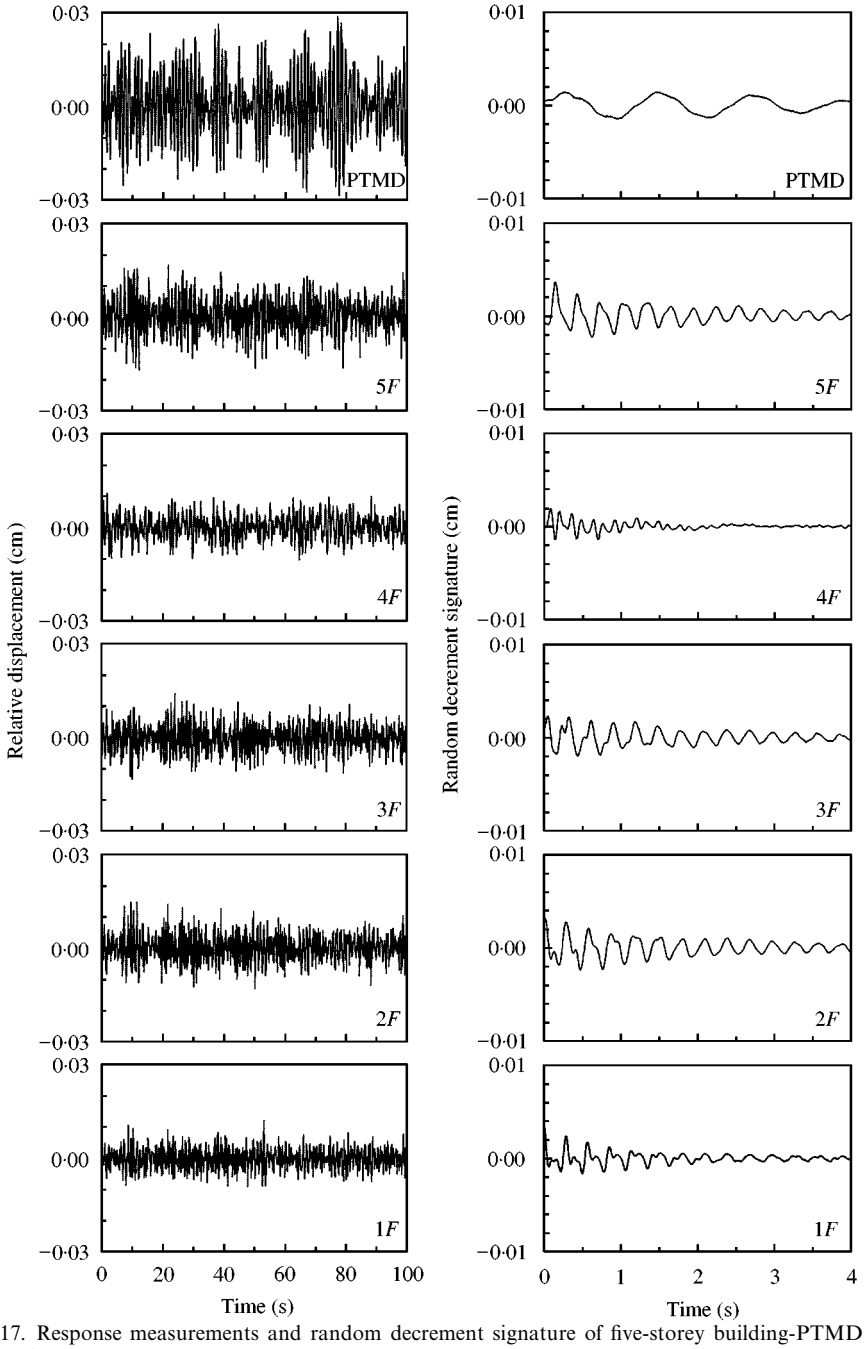

Figure 17. Response measurements and random decrement signature of five-storey building-PTMD system (NSR = 20%).

The first two modal dampings increase to about 7% due to the presence of PTMD, and thus, the dynamic responses due to El Centro (S00E) earthquake are reduced, as shown in Figure 19 and Table 5. The predicted relative displacement and absolute acceleration at the fourth floor (unmeasured location) and fifth floor (measured location) of the building with

TABLE 4

Identified modal frequencies and damping ratios for five-storey building-PTMD system

	Natural frequency (Hz)					Damping ratio (%)				
		NSR = 0%		NSR = 20%			NSR = 0%		NSR = 20%	
Mode	True	Full	Partial	Full	Partial	True	Full	Partial	Full	Partial
1	0·778	0·778 (0·0%)	0·731 (−6·0%)	0·774 (−0·6%)	0·745 (−4·2%)	7·663	8·204 (+7%)	8·963 (+17%)	6·779 (−12%)	6·734 (−12%)
2	0·987	0·970 (−1·7%)	0·931 (−5·7%)	0·990 (+0·3%)	0·955 (−3·2%)	7·198	6·244 (−13%)	3·900 (−46%)	7·263 (−1%)	5·598 (−22%)
3	3·376	3·351 (0·5%)	3·358 (−0·5%)	3·359 (−0·5%)	3·361 (−0·4%)	2·162	1·686 (−22%)	1·796 (−17%)	1·866 (−14%)	2·051 (−5%)
4	7·108	7·118 (+0·1%)	7·132 (0·3%)	7·122 (+0·2%)	7·136 (+0·4%)	2·032	1·493 (−27%)	1·496 (−26%)	1·573 (−23%)	1·686 (−17%)
5	10·657	10·690 (−0·3%)	—	—	—	2·007	1·983 (−1%)	—	—	—
6	12·728	12·215 (−4·0%)	—	—	—	2·001	1·980 (−1%)	—	—	—

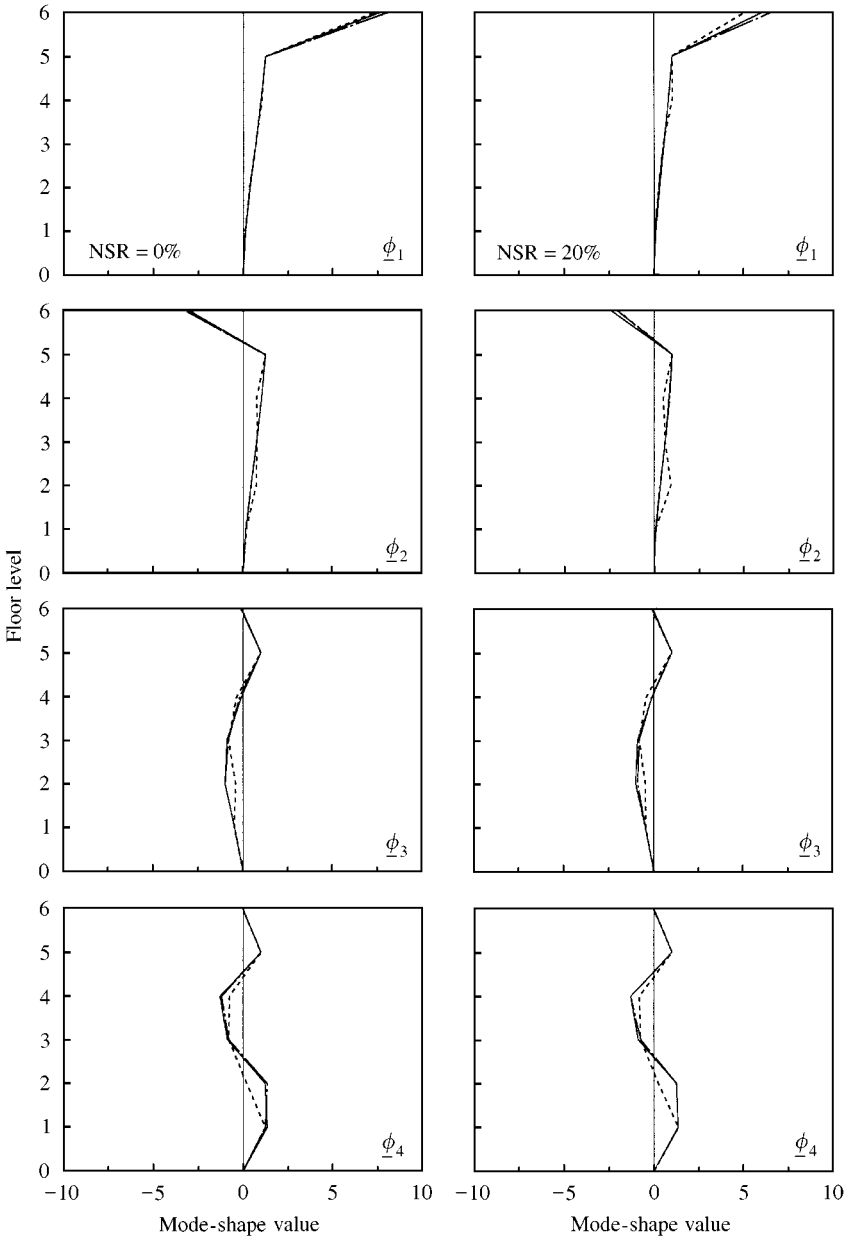

Figure 18. Calculated versus true mode shapes of five-storey building-PTMD system: ———, true; —·—, full measurements; - - - - - - - - -, 1, 3, 5F, PTMD measurements.

PTMD are given in Figure 20. The results show both responses at measured and unmeasured locations were predicted accurately. Since the contribution of higher mode response for acceleration is important and the system identification error in higher modal parameters is larger than that of fundamental mode, the predicted relative displacements are more precise than those for absolute accelerations. Also, the optimal PTMD is effective in reducing peak and root-mean-square (rms) responses, as expected.

TABLE 5

Response estimation under El Centro Earthquake with and without PTMD

Case of response	Peak response			rms response		
	Without PTMD	With PTMD		Without PTMD	With PTMD	
		True	NSR = 20%		True	NSR = 20%
4F relative displacement (cm)	16·47	10·84 (− 34·1%)	11·14 (− 32·4%)	4·29	2·05 (− 52·2%)	2·09 (− 51·3%)
5F relative displacement (cm)	20·49	13·69 (− 33·2%)	14·04 (− 31·5%)	5·27	2·52 (− 52·2%)	2·61 (− 50·5%)
4F absolute acceleration (g)	0·73	0·51 (− 30·1%)	0·60 (− 17·8%)	0·150	0·079 (− 47·3%)	0·092 (− 38·7%)
5F absolute acceleration (g)	0·96	0·79 (− 17·71%)	0·85 (− 11·5%)	0·198	0·120 (− 39·4%)	0·134 (− 32·3%)

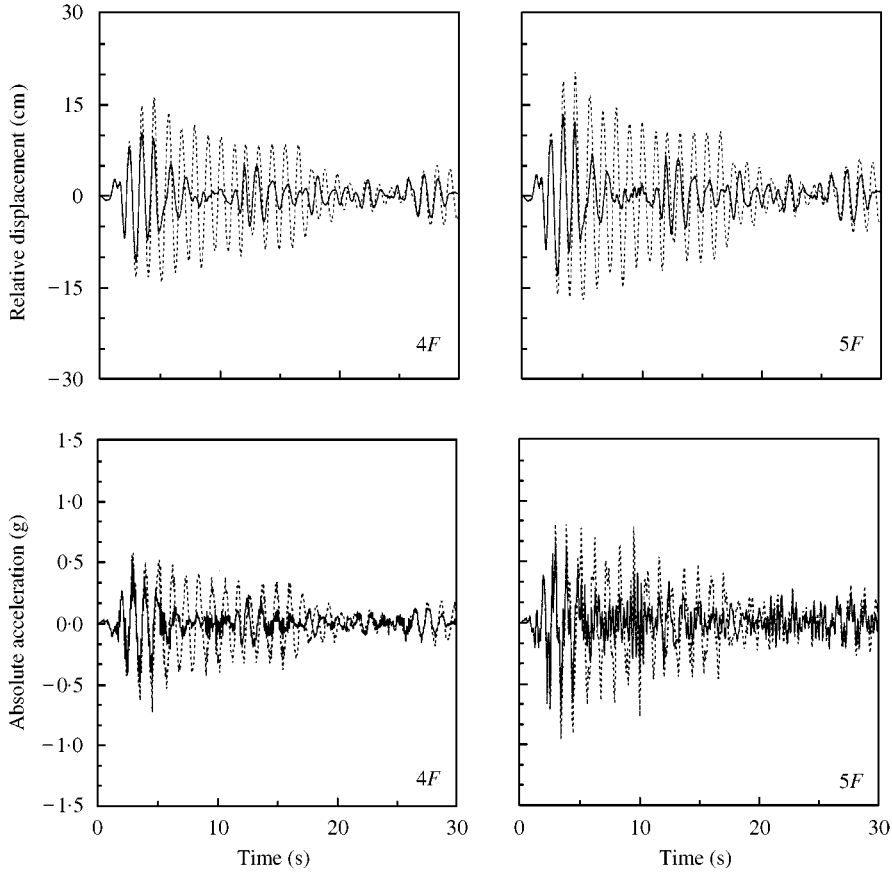

Figure 19. Calculated floor displacement and acceleration of five-storey building with and without PTMD under 1940 El Centro earthquake: -------, w/o PTMD; ——, with PTMD.

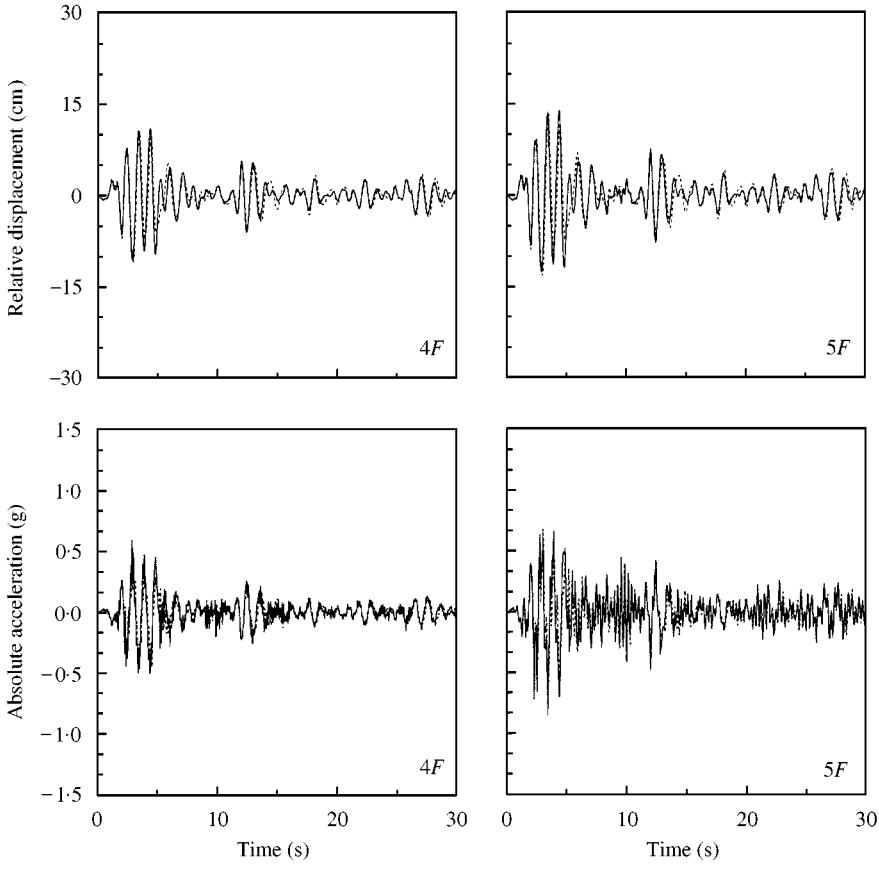

Figure 20. Predicted floor displacement and acceleration response of five-storey building-PTMD system under 1940 El Centro earthquake: ----------, true; ———, NSR = 20%.

5. CONCLUSIONS

In this paper, the extended random decrement method combined with the Ibrahim time domain identification technique was used to identify the modal properties for buildings with and without PTMDs based on only a few floor response measurements. An interpolation method was developed to estimate the mode shape values for the locations without measurement. Structural seismic responses were also predicted. Numerical simulation results using a five-storey building with optimal PTMD demonstrated that the proposed system identification techniques can identify system dominant modal parameters accurately even with high closed-space frequencies and noise contamination. A small number of response measurements, no requirement for input excitation measurements and simple on-line calculation make the proposed system identification techniques favorable to real implementation. In addition, the PTMD vibration control philosophy was introduced and the effectiveness of PTMD on real-ground motion was investigated to indicate the overall performance of this control device. It was proved that PTMD is useful because system damping increases after its implementation.

ACKNOWLEDGMENTS

This work was supported by the National Science Council of the Republic of China under Contracts No. NSC 85-2621-P-005-006 and NSC 86-2621-P-005-006. These supports are greatly appreciated. The authors would like to thank the reviewers for their constructive comments that improved the quality of the paper.

REFERENCES

1. M. GU, H. F. XIANG and A. R. CHEN 1994 *Journal of Wind Engineering and Industrial Aerodynamics* **51**, 203–213. A practical method of passive TMD for suppressing wind-induced vertical buffeting of long-span cable-stayed bridges and its application.
2. M. SATAREH and R. D. HANSON 1992 *ASCE Journal of Structural Engineering* **118**, 723–740. Tuned mass dampers for balcony vibration control.
3. M. SATAREH and R. D. HANSON 1992 *ASCE Journal of Structural Engineering* **118**, 741–762. Tuned mass dampers to control floor vibration from humans.
4. C. C. LIN, C. M. HU, J. F. WANG and R. Y. HU 1994 *Journal of the Chinese Institute of Engineers* **17**, 367–376. Vibration control effectiveness of passive tuned mass dampers.
5. C. C. CHANG 1999 *Engineering Structures* **21**, 454–463. Mass dampers and their optimal designs for building vibration control.
6. J. P. DEN HARTOG 1956 *Mechanical Vibration*. New York: McGraw-Hill.
7. P. H. WIRSCHING and G. W. COMBELL 1974 *Earthquake Engineering and Structural Dynamics* **2**, 303–312. Minimal structural response under random excitation using the vibration absorber.
8. R. W. LUFT 1979 *ASCE Journal of the Structural Division* **105**, 2766–2772. Optimal tuned mass dampers for buildings.
9. G. B. WARBURTON and E. O. AYORINDE 1980 *Earthquake Engineering and Structural Dynamics* **8**, 197–217. Optimal absorber parameters for simple systems.
10. G. B. WARBURTON 1982 *Earthquake Engineering and Structural Dynamics* **10**, 381–401. Optimum absorber parameters for various combinations of response and excitation parameters.
11. H. C. TSAI 1996 *Earthquake Engineering and Structural Dynamics* **25**, 1–13. Envelope of Green's function for structural response with slightly detuned vibration absorbers.
12. Y. FUJINO and M. ABE 1993 *Earthquake Engineering and Structural Dynamics* **22**, 833–854. Design formulas for tuned mass dampers based on a perturbation technique.
13. F. SADEK, B. MOHRAZ, A. W. TAYLOR and R. M. CHUNG 1997 *Earthquake Engineering and Structural Dynamics* **26**, 617–635. A method of estimating the parameters of tuned mass dampers for seismic applications.
14. R. VILLAVERDE 1985 *Earthquake Engineering and Structural Dynamics* **13**, 33–42. Reduction in seismic response with heavily-damped vibration absorbers.
15. M. N. S. HADI and Y. ARFIADI 1998 *ASCE Journal of the Structural Engineering* **124**, 1272–1280. Optimum design of absorber for m.d.o.f. structures.
16. A. CAROTT and E. TURCI 1999 *Applied Mathematical Modeling* **23**, 199–217. A tuning criterion for the inertial tuned damper. Design using phasors in the Argand–Gauss plane.
17. M. C. CONSTANTINOU, T. T. SOONG and G. F. DARGUSH 1998 *Multidisciplinary Center for Earthquake Engineering Research, U.S.A., Monograph Series*, Vol. 1. Passive energy dissipation systems for structural design and retrofit.
18. Y. L. XU and K. C. S. KWOK 1994 *ASCE Journal of Structural Engineering* **120**, 747–764. Semi-analytical method for parametric study of tuned mass dampers.
19. R. VILLAVERDE 1994 *Proceeding of the* 1*st World Conference on Structural Control*, *Los Angels*, *CA*, *U.S.A.*, Vol. 1, Wp4-133–Wp4-122. Seismic control of structures with damped resonant appendages.
20. R. RANA and T. T. SOONG 1998 *Engineering Structures* **20**, 193–204. Parametric study and simplified design of tuned mass dampers.
21. A. J. CLARK 1998 *Proceeding of the* 9*th World Conference on Earthquake Engineering*, *Tokyo/Kyoto*, *Japan*, **5**, 779–784. Multiple passive tuned mass damper for reducing earthquake induced building motion.
22. K. XU and T. IGUSA 1992 *Earthquake Engineering and Structural Dynamics* **21**, 1059–1070. Dynamic characteristics of multiple sub-structures under closely spaced frequencies.

23. H. YAMAGUCHI and N. HARNPORNCHAI 1993 *Earthquake Engineering and Structural Dynamics* **22**, 51–62. Fundamental characteristics of multiple tuned mass dampers for suppressing harmonically forced oscillation.
24. A. KAREEM and S. KLINE 1995 *ASCE Journal of Structural Engineering* **12**, 348–361. Performance of multiple tuned mass dampers under random loading.
25. Y. L. XU, B. SAMILI and K. C. S. KWOK 1992 *ASCE Journal of Engineering Mechanics* **118**, 20–39. Control of along-wind response of structures by mass and liquid dampers.
26. Y. L. XU, K. C. S. KWOK, and B. SAMILI 1992 *Journal of Wind Engineering and Industrial Aerodynamics* **40**, 1–32. Control of wind-induced tall building vibration by tuned mass dampers.
27. A. KAWAGUCHI, A. TERAMURA and Y. OMOTO 1992 *Journal of Wind Engineering and Industrial Aerodynamics* **41–44**, 1949–1960. Time history response of a tall building with a tuned mass damper under wind force.
28. J. M. UENG, C. C. LIN and P. L. LIN 2000 *Computers and Structures* **74**, 667–686. System identification of torsionally coupled buildings.
29. H. FRAHM 1911 *U.S. Patent* **989–958**. Device for damping vibrations of bodies.
30. S. R. IBRAHIM and R. S. PAPPA, 1982 *AIAA Journal of Spacecraft and Rockets* **19**, 459–465. Large model survey testing using the time domain identification technique.

APPENDIX A: NOMENCLATURE

$\mathbf{1}$	vector with each element of 1
$\mathbf{A}$	Ibrahim system matrix
$\mathbf{C}$	damping matrix of the primary structure-PTMD system
$\mathbf{C}_p$	damping matrix of the primary structure
c_s	PTMD's damping coefficient
$E[\eta_1^2]_{\text{PTMD}}$	mean-square displacement response of the first mode of the primary structure with PTMD
$E[\eta_1^2]_{\text{NOPTMD}}$	mean-square displacement response of the first mode of the primary structure without PTMD
$\mathbf{f}_{\text{TMD}}$	loading vector acting on the primary structure by PTMD
$\lvert H_{\eta 1 \ddot{x}_g}(\omega)\rvert_{\text{PTMD}}$	magnitude of the first mode transfer function of primary structure with PTMD
$\lvert H_{\eta 1 \ddot{x}_g}(\omega)\rvert_{\text{NOPTMD}}$	magnitude of the first mode transfer function of primary structure without PTMD
$\mathbf{K}$	stiffness matrix of the primary structure-PTMD system
$\mathbf{K}_p$	stiffness matrix of the primary structure
k_s	PTMD's stiffness coefficient
$\mathbf{M}$	mass matrix of the primary structure-PTMD system
$\mathbf{M}_p$	mass matrix of the primary structure
m_j^*	jth generalized modal mass of the primary structure
m_s	PTMD's mass
N_s	superposition times of random decrement method process
R_{aE}	mean-square acceleration response ratio of primary structure
R_{dE}	mean-square displacement response ratio of primary structure
$R_{dE,1}$	mean-square displacement response ratio of the first mode of the primary structure
$(r_f)_{opt}$	optimal PTMD frequency ratio
$S_{\ddot{x}_g}(\omega)$	power spectrum of earthquake ground acceleration
t_d	duration of random decrement signature
$\mathbf{u}$	location vector of PTMD
$u(t)$	response measurement
u_s	trigger level of the random decrement method process
v	PTMD's stroke
$\mathbf{X}$, $\hat{\mathbf{X}}$	Ibrahim response matrices
$\mathbf{x}(t)$	displacement vector of the primary structure-PTMD system
x_i	displacement of the ith floor of the primary structure
$\ddot{x}_g(t)$	earthquake ground acceleration
$\mathbf{x}_p(t)$	displacement vector of the primary structure relative to base
$x_s(t)$	displacement of PTMD relative to base
Γ_j	jth modal participation factor
$\delta(\tau)$	random decrement signature

η_j	jth modal displacement of the primary structure
$\mathbf{\Lambda}$	Ibrahim exponential function matrix
λ_k	kth complex eigenvalue
μ	mass ratio of PTMD to the total mass of primary structure
$(\mu_1)_{opt}$	optimal PTMD mass ratio
ξ_g	site damping ratio
ξ_j	jth modal damping ratio of primary structure
ξ_p	damping ratio of primary structure
ξ_s	PTMD's damping ratio
$(\xi_s)_{opt}$	optimal PTMD damping ratio
ω_g	site dominant frequency
ω_j	jth modal frequency of primary structure
ω_p	natural frequency of primary structure
ω_s	PTMD's natural frequency
ϕ_{ij}	ith value of the jth mode shape of the primary structure
$\boldsymbol{\phi}_j$	jth mode shape vector of primary structure
φ_{lk}	kth complex mode shape at location l
$\mathbf{\Psi}, \hat{\mathbf{\Psi}}$	Ibrahim complex mode shape matrices